Scrutinizing interlaminar fatigue loading cycle in composites using acoustic emission technique: Stress ratio influence on damage formation

Ferreira Motta Junior, R.; Alderliesten, R.C.; Shiinoc, Marcos Yutaka; Cioffia, Maria Odila Hilário; Voorwald, Herman Jacobus Cornelis

DOI
10.1016/j.compositesa.2020.106065

Publication date
2020

Document Version
Final published version

Published in
Composites Part A: Applied Science and Manufacturing

Citation (APA)
Ferreira Motta Junior, R., Alderliesten, R. C., Shiinoc, M. Y., Cioffia, M. O. H., & Voorwald, H. J. C. (2020). Scrutinizing interlaminar fatigue loading cycle in composites using acoustic emission technique: Stress ratio influence on damage formation. *Composites Part A: Applied Science and Manufacturing*, *138*, Article 106065. https://doi.org/10.1016/j.compositesa.2020.106065

Composites Part A 138 (2020) 106065

Contents lists available at ScienceDirect

Composites Part A

journal homepage: www.elsevier.com/locate/compositesa

Scrutinizing interlaminar fatigue loading cycle in composites using acoustic emission technique: Stress ratio influence on damage formation

Roberto Ferreira Motta Jr.[a,*], René Alderliesten[b], Marcos Yutaka Shiino[c], Maria Odila Hilário Cioffi[a], Herman Jacobus Cornelis Voorwald[a]

[a] São Paulo State University (Unesp), Materials and Technology Department, Fatigue and Aeronautic Materials Research Group, Guaratinguetá, SP, Brazil
[b] Aerospace Structures and Materials Department, Faculty of Aerospace Engineering, Delft University of Technology, P.O. Box 5058, 2600 GB Delft, the Netherlands
[c] São Paulo State University (Unesp), Institute of Science and Technology, São José dos Campos, SP, Brazil

ARTICLE INFO

Keywords:
Laminates
Delamination
Fatigue
Acoustic emission

ABSTRACT

Current models for delamination propagation prediction in fiber-reinforced polymer (FRP) composites exhibit limitations to explain the physics underlying the mechanisms of damage formation in fatigue. In order to contribute in this field, this research focuses on the study of damage development within a single loading cycle of FRP double cantilever beam specimens under different stress ratios (R). The acoustic emission technique was used to investigate damage propagation. Results showed that under high R-ratios, the load cycle spends an increased time above the threshold energy (U_{th}). This time difference affects the damage distribution within a single loading cycle. Furthermore, the steady-state delamination propagation was influenced by the R-ratio variation due to the modification of the external work applied to the specimen.

1. Introduction

Fiber-reinforced polymer (FRP) composites have a great potential to replace metals in applications that require lighter components and structures, since these materials are capable of reaching high in-plane properties of specific strength and stiffness. However, FRPs exhibit a low interlaminar strength, which leads to delamination and hinders its use in primary structural applications. Therefore, extensive research has been conducted to understand quasi-static and fatigue delamination growth in FRPs over the past decades.

Many of these works have focused on the development of fatigue delamination growth (FDG) models aiming to predict the lifetime of FRP structural components under cyclic loading. As examples, Amaral et al. used the physical strain energy release rate (SERR – G) basis theory to compare mode I crack extensions in fatigue and quasi-static loading, and concluded that the SERR depends on the damage state of the fracture surface [1]. Zhang et al. developed a novel double-load-envelop numerical method to predict fatigue delamination propagation in composite laminates [2]. The works of Yao et al. [3] and Jones et al. [4] obtained the fatigue resistance curves of FRPs using the Hartman–Schijve equation, which is a phenomenological approach capable of performing lifetime predictions. Another recurrent focus of the research regarding delamination is the study of the micro-mechanisms associated with the process. Khan et al. [5] and Varandas et al. [6] studied the micro-mechanisms developed in mode I delamination propagation, and Bertorello et al. [7] evaluated the influence of the matrix type on delamination growth, which exemplifies the considerable potential of the micro-mechanical analysis to increase the knowledge regarding the delamination process.

In order to guarantee the reliability of composite structures, it is essential to comprehend the physics underlying their fatigue behavior, to enable the development of FDG models capable of estimating reliable component lifetimes and maintenance periods. A large number of FDG models has been developed so far, but the understanding of the fracture process' underlying physics is still lacking [8,9]. The knowledge of the micro-mechanisms involved in the delamination propagation increases the understanding of the phenomenon and enables physical explanations. However, few researchers have used micro-mechanical analysis to develop FDG models. In order to develop an FDG prediction model based on physical concepts, the form of the equation should be explained by the mechanisms observed during the phenomenon, which means that micromechanical models should receive more attention.

In literature, a limited number of micromechanical models for FDG were found [10]. Khan et al. [11] developed a model based on damage

* Corresponding author at: São Paulo State University (Unesp), Materials and Technology Department, Fatigue and Aeronautic Materials Research Group, Guaratinguetá, SP 12516-410, Brazil.
E-mail address: roberto.motta@unesp.br (R. Ferreira Motta Jr.).

https://doi.org/10.1016/j.compositesa.2020.106065
Received 20 May 2020; Received in revised form 30 July 2020; Accepted 1 August 2020
Available online 05 August 2020
1359-835X/

mode features observed on fracture surfaces by scanning electronic microscopy (SEM). In the work of Khan, the matrix' cohesive failure was associated with hackle formation, and the fiber-matrix decohesion assessed by the presence of striations in the fiber imprints. Brighenti et al. [12] used the fracture mechanics approach to describe fiber debonding and simulated progressive fiber detachment. Indeed, both models were based on micro-mechanisms developed during FDG but neglected relevant mechanisms of the delamination process, such as fiber bridging, fiber failure, and damage formation ahead of the crack tip. Khan et al. [11] justified that both fiber failure and fiber bridging formation were not considered in the model because they are mechanisms developed behind the crack tip. However, Yao et al. [13] showed that these mechanisms also contribute to the material's resistance, since strain energy is released when bridging fibers fail or are pulled out of the matrix.

The creation of new micromechanical models relies on knowledge of how the damage is created over a single loading cycle and the correct quantification of this damage [9,10]. There is a consensus on using the macroscopic crack length to quantify the damage developed during the fatigue process, which is not capable of representing the physical damage created within a single loading cycle. The use of the one-dimensional crack length concept to quantify the damage created in FDG has been shown to be efficient for engineering purposes. However, considering a scientific point of view, there are some problems and limitations in using the macroscopic crack length to quantify physical fatigue damage.

Considering typical fatigue tests with double cantilever beam (DCB) specimens, a crack propagates during the loading cycles, and a camera captures images of the delamination profile in pre-determined time intervals. This technique of monitoring the delamination length presents some limitations. The limited resolution of the optical lenses detecting microscopic details of the delamination increment inhibits analyses of how the damage propagates within a single load cycle [10]. Besides, the fact that the crack propagation is monitored only at the specimen's edge means it is not possible to observe damage propagation inside the specimen. Therefore, as a consequence of these conditions, the macro-crack length is an average over the width, the time scale, and the topography, leading to the following approximations: a straight crack front, a constant propagation rate for multiple consecutive loading cycles, and a perfectly plane topography, respectively [11].

Moreover, the damage quantification using the crack length does not consider the micro-crack formation ahead of the crack tip [14]. Thus, although the crack length proved to be a good approximation of the damage in progress under fatigue, it cannot provide a full understanding of the phenomenon, which hinders further developments.

1.1. The use of acoustic emission (AE) technique to quantify physical damage in fatigue

In order to thoroughly understand the mechanisms of damage formation in fatigue, non-destructive evaluation (NDE) techniques have gained more attention. The acoustic emission (AE) technique is one of the NDE techniques most frequently used to study damage formation in composites [15–18]. One of the main reasons for its application is the fact that the AE is a passive technique, which means that the source of the acoustic signal is located inside the material, enabling the material's behavior monitoring under loading conditions [15]. The source of the AE signals can be related to damage nucleation and propagation, plastic deformation, or even internal friction [19]. The development of these damage mechanisms inside the material causes sudden internal displacements combined with spatial crack surface oscillations originating acoustic waves. Once originated, these acoustic signals have their features affected by the wave propagation until their detection on the material's surface by the piezoelectric sensor [20]. Therefore, the correct interpretation of the signals detected by the AE technique relies on a complete understanding of the wave features, also referred to as AE parameters.

Some AE parameters, such as the peak amplitude, peak frequency, energy, duration, counts, and rise time, have been used to interpret acoustic signals and study the damage formation process in FRPs. Most of the works have focused on damage onset detection, damage location, damage identification, and studies related to the remaining useful life and residual strength of composite structures [19]. Barile et al. used the sentry function to relate the acoustic energy with the strain energy released by the material during delamination propagation in [15] and investigated the effect of the number of plies, fiber orientation, and thickness of carbon fiber reinforced polymer (CFRP) composites on the AE parameters in [21]. Fatih et al. [22] evaluated the frequency bandwidth of typical damage modes of the delamination propagation in FRP, such as fiber breakage and matrix cracking. Pascoe et al. [10] studied the damage formation in the course of a single loading cycle using the AE technique and concluded that the damage onset within a fatigue cycle only happens if a strain energy threshold is overcome.

As demonstrated, a substantial number of researchers have used the AE technique to evaluate delamination in FRP [10,23–28]. However, only a few of them focused on the study of damage formation within a single loading cycle. Consequently, the damage formation process within a single loading cycle still presents some interesting questions. For example, it is unknown if the entire load cycle is relevant to FDG prediction models, and if it is not, which portion of the loading cycle should be considered? Is there any stochastic process acting on fatigue delamination growth? Moreover, does the R-ratio have any influence in the region of the cycle where the damage occurs?

In order to address these questions, this research focuses on explaining how the damage propagates within a single loading cycle. To accomplish this, the mode I FDG of CFRP composites was monitored using the AE technique, and the damage distribution within a loading cycle was investigated.

2. Materials and methods

2.1. Test set-up of mode I fatigue delamination propagation, specimen preparation, and the AE equipment and settings

Six DCB specimens of CFRP, namely: FT-1, FT-2, FT-3, FT-4, FT-5, and FT-6 were prepared following the guidelines given in ASTM D5528-13 [29], as illustrated in Fig. 1a.

The specimens were obtained from two CFRP laminates processed via resin transfer molding (RTM) with the same pre-form but with different fiber volume fractions (FVF), using as the matrix a monocomponent PRISM™ EP2400 epoxy system. The pre-form was composed of eight plies of bidiagonal carbon fiber stitched fabrics, stacked up in an orthotropic $[90^{\circ}/0^{\circ}]_{4S}$ lay-up, resulting in the laminates 1 and 2 with the following FVF and thickness: 49.6% (± 2.7), 4.01 mm (± 0.17) and 54.7% (± 1.6), 3.37 mm (± 0.16), respectively. The FVF measurements were obtained by acid digestion following ASTM D3171-15 [30]. The fabrics were supplied by SAERTEX, comprised of Hexcel IM7 GP carbon fibers, and stitched with PES SC yarns.

An inserted film of polytetrafluoroethylene with 13 μm thickness was added between 0°/0° mid-plane interface to produce a pre-crack of approximately 50 mm (measured from the load line until pre-crack tip). One edge of each specimen was coated with type-writer correction fluid (white color) to promote a better visualization of the crack tip.

The specimens FT-1, FT-2, and FT-3 were obtained from laminate 1, whereas the specimens FT-4, FT-5, and FT-6 were obtained from laminate 2. All the specimens were tested in mode I under fatigue with displacement-controlled conditions following the guidelines of ASTM D6115-97 [31], and different loading ratios: R = 0 (FT-1 and FT-4), R = 0.5 (FT-2 and FT-5), and R = 0.8 (FT-3 and FT-6). The R-ratio varied regarding the minimum displacement (d_{min}), keeping the maximum displacement (d_{max}) constant for all the tests. The d_{max} used in the fatigue tests was determined based on quasi-static test results. The

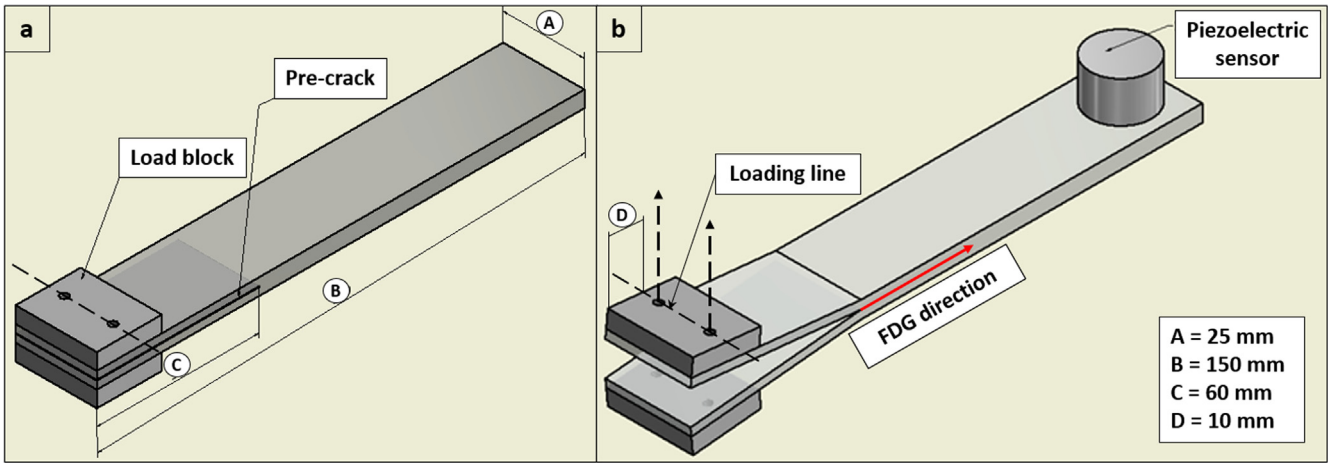

Fig. 1. (a) DCB specimen dimensions according to ASTM D5528-13, (b) position of the piezoelectric sensor used to detect the hits in the AE technique. (For interpretation of the references to colour in this figure legend, the reader is referred to the web version of this article.)

Table 1
The values of maximum and minimum displacement used in each fatigue test with their respective R-ratio.

Specimen	Maximum displacement (mm)	Minimum displacement (mm)	R-ratio
FT-1	8.00	0.00	0.0
FT-2	8.00	4.00	0.5
FT-3	8.00	6.40	0.8
FT-4	9.50	0.00	0.0
FT-5	9.50	4.75	0.5
FT-6	9.50	7.60	0.8

average displacement of the maximum load in the quasi-static tests was obtained for both laminates, and 75% of this value was taken as d_{max}. The values of d_{max} and d_{min} of the fatigue tests are presented in Table 1.

The tests were performed by an MTS 15 kN servo-hydraulic fatigue machine equipped with a load-cell of 1 kN under a loading frequency of 1 Hz (low frequency to reduce noise generation). A camera was positioned facing the edge of the specimen to monitor the crack length with the acquisition rate of one picture every 60 cycles.

The AE system used in the tests was an 8-channel AMSY-6 Vallen with four parametric inputs. A high sensitivity wide-band piezoelectric sensor (AE1045S) with an operating frequency ranging between 100 and 900 kHz was clamped on one of the specimen's extremities (Fig. 1b) to capture the AE events (called "hits") originated during the fatigue tests. The sensor was connected to an external 34 dB pre-amplifier with a band-pass filter of 20–1200 kHz. Grease was used as a coupling fluid to eliminate the effect of the material's surface roughness, affecting the piezoelectric sensor performance in recording the resonances and reverberations [15,32]. The pencil lead break procedure was used to ensure a proper conductivity between the specimen's surface and the sensor [33]. The amplitude threshold for the recorded signals was set at 50 dB, and the tests were performed with a sampling rate of 2 MHz [10,34]. The entire setup was integrated to synchronize the parameters for data reduction: load, displacement, and AE signals.

2.2. Methodology of damage distribution analysis within a single loading cycle

Current prediction models for FDG assume in their analysis that the delamination propagation rate is constant within a single loading cycle, which is an approximation and requires further investigations. The methodology used in this work to study damage distribution within a single loading cycle is presented. The cycles were divided into seven regions with an equal time interval, as illustrated in Fig. 2. The moment

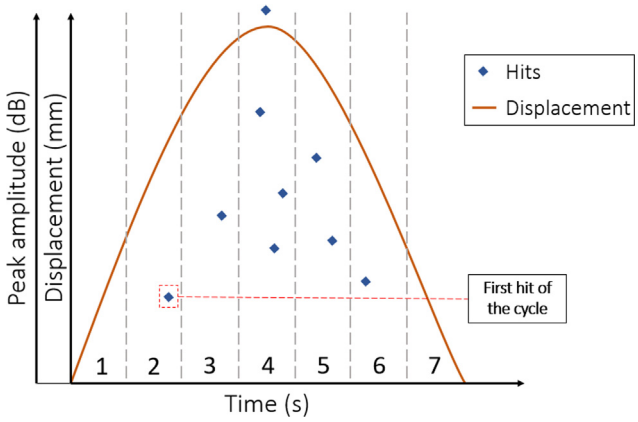

Fig. 2. Illustrative scheme of the distribution of the hits over a single load cycle. (For interpretation of the references to colour in this figure legend, the reader is referred to the web version of this article.)

the damage occurred within the loading cycle is known because hits and displacement are time-correlated. Therefore, it is possible to count how many hits were detected in each pre-determined region of the loading cycle during the fatigue tests.

The decision to divide the cycle into seven regions was taken based on two restricting factors. First, an odd number of regions is required to guarantee that the acoustic signals detected at the moment the cycle reaches d_{max} are always in the same region (region four), and not shifting between two adjacent regions, which is essential considering that most of the damage is expected to develop surrounding d_{max}. Second, the number of regions (divisions) cannot be high, aiming to avoid a relevant influence of the time-delay between damage event and signal detection in the results.

Once a damage event occurs, an acoustic wave is created, and the signal has to propagate until reaching the piezoelectric sensor. Thus, there is a delay between damage formation and signal detection. The time interval of each region presented in Fig. 2 is 1/7 s, considering that one cycle takes 1 s to develop. Taking into account the pre-crack length and the position of the piezoelectric sensor (shown in Fig. 1), and assuming that the sound propagation speed in CFRP is about 3 mm/μs [35], a maximum time-delay of 33.3 μs is estimated, representing about 0.023% of the time interval of a single region depicted in Fig. 2. Since the time-delay in data acquisition is low compared to the time interval of a single region of the cycle, the time-delay was neglected in the data reduction.

The position of each hit within a single loading cycle and its

respective region were obtained for the first five hundred cycles of each test, and the percentage of hits detected in each region was calculated. Only five hundred cycles were considered in the results to reduce noise detection. The assessment of more cycles means more time for delamination propagation, resulting in longer crack lengths and, consequently, more noise from friction. Aiming to evaluate the damage onset in each cycle, the first hit detected (as detailed in Fig. 2) was considered the damage propagation onset.

3. Results and discussions

Sections 3.1, 3.2, 3.3, and 3.4 present the analysis of damage propagation and damage distribution in the course of a single loading cycle using the AE technique. With these results, some physical explanations concerning the damage formation mechanisms can be given.

3.1. R-ratio variation influence on damage formation within a single loading cycle

The R-ratio influence over the micro-mechanisms developed during FDG must be understood to enable the development of micro-mechanical models. The R-ratio variation changes the external work applied to a specimen, which changes the delamination growth rate, but how it changes the distribution of the damage within a single loading cycle is unknown. Therefore, aiming to understand the R-ratio influence on damage distribution fully, Figs. 3 and 4 show the damage distribution within a single loading cycle during the first five hundred cycles of each fatigue test. The specimens were obtained from two laminates with different FVF to verify if the damage distribution behavior is the same when the FVF is increased since laminates with high FVF are often used in structural applications.

Specimens FT-1 and FT-4 were tested with an R-ratio of zero, which means a d_{min} of zero, leading to a total crack closure in each cycle. This process of total closure and opening of the fractured surfaces causes internal friction that is a source of noise. Analysis of Fig. 3a and d show a considerable incidence of hits in sections 6 and 7 of the cycle, indicating a substantial amount of noise originated by crack closure friction, and a lower incidence of hits originated by crack opening friction in section 1 of the cycle, which is in agreement to more intense friction during crack closure.

The friction noise observed in the fatigue tests of specimens FT-1 and FT-4 is better observed in details a, b, c, and d of Fig. 4a and d. Fig. 4 presents the position of the hits within the loading cycle and the amplitude of each signal. Both specimens FT-1 and FT-4 showed a very similar behavior, as can be seen in Fig. 4a and d. A small cluster of hits is observed in section 1 of the cycle of both specimens (details a and c). The proximity of the fractured surfaces and the low strain energy accumulated in section 1 of the specimens tested with an R-ratio of 0 leads to the conclusion that the source of these signals was friction of the fracture surfaces during the crack opening. A more relevant cluster of hits is observed in sections 6 and 7 of the cycle of both specimens (details b and d). The source of these signals was the friction of the fracture surfaces during the crack closure, based on the proximity between the fracture surfaces and the low strain energy level of the specimens in these sections.

Considering that the hits detected in sections 1, 6, and 7 of the specimens FT-1 and FT-4 were mostly friction noise, the hits corresponding to damage formation are concentrated in sections 2, 3, 4, and 5 of the cycle (Fig. 4a and d). These regions possess higher values of displacement and external load applied to the specimen. Consequently, a higher amount of strain energy is accumulated in the specimen, allowing damage development.

Fig. 3a and d showed a higher incidence of hits in section 3, indicating that more hits originated by damage mechanisms were detected before the cycle reaches d_{max} (condition of maximum strain energy accumulation within the loading cycle). The hits corresponding to damage formation of specimens FT-1 and FT-4 can be observed in Fig. 4a and d, respectively, as a unique hit cluster in sections 2, 3, 4, and 5 of the cycle. This cluster of hits starts in section 2 with low amplitude hits, then the amplitude of the hits presented an increase until reach a maximum in section 4 and a slight reduction in section 5 where the cluster ends. This variation in the amplitude of the signals in different sections of the cycle can indicate that different damage modes are trigged in different sections of the cycle. This statement is based on the fact that different damage modes require different amounts of energy to develop, and different sections of the cycle present different levels of strain energy accumulation. However, a proper damage mode identification requires the assessment of more AE parameters and must be conducted in future works. The bandwidth range used in the AE set up in this study detected hits from internal friction, which complicated the analysis of the results. In future works, the frequencies associated to friction hits must be determined first, and then a bandpass filter above this value set to avoid the detection of noise from friction in the results.

The specimens tested with an R-ratio of 0.5 (Fig. 3b and e) presented a relevant reduction of the friction noise due to the increase of d_{min}, leading to a better visualization of damage formation. However, a small cluster of hits that might be attributed to crack closure friction was still observed in section 7 of specimen FT-5 in Fig. 4e. As observed in specimens FT-1 and FT-4 (Fig. 3a and d), specimens FT-2 and FT-5 (Fig. 3b and e) also showed a concentration of hits in sections 3 and 4 surrounding d_{max}, but hits indicating damage formation were observed in all sections. Moreover, an increasing trend in the hit amplitude surrounding d_{max} was observed in the results of specimens FT-2 and FT-5 (Fig. 4b and e), similar to specimens FT-1 and FT-4 (Fig. 4a and d).

The specimens FT-3 and FT-6 were tested with an R-ratio of 0.8 (Fig. 3c and f). The R-ratio increase reduced the hit concentration around d_{max} compared to the results of the specimens tested with the R-ratios of 0 and 0.5. This more homogeneous damage distribution behavior is a consequence of the increase of d_{min} (condition of minimum strain energy state). Keeping d_{max} (condition of maximum strain energy state) constant and increasing d_{min}, the cyclic strain energy is reduced, while the monotonic strain energy of the specimen is increased. Consequently, the specimen will be continuously at a high level of strain energy. On the other hand, the reduction of the cyclic energy applied to the specimen led to a reduction in the number of hits detected, indicating a lower delamination propagation rate, as depicted in Fig. 4.

According to the work of Pascoe et al. [10], there is a threshold value of energy that must be overcome to enable damage formation in each cycle, called G_{th}. Considered this, the damage mechanisms detected by the AE system during the tests of all the specimens occurred when the specimen had a strain energy state (G) above G_{th}. The concept of G used by Pascoe in his work stems from fracture mechanics. In contrast, in the present work, the discussions will be performed based on the definition of G as physics-based characterization of resistance ($G = dU/dA$), i.e. the result of crack growth, in which U is the internal strain energy stored in the specimen, and A is the area corresponding to the crack propagation. Therefore, the strain energy threshold required for damage onset within a fatigue cycle will be referred to as U_{th} instead of G_{th} in the following discussions.

The total strain energy stored in the specimen within a single loading cycle (U_{tot}) can be divided into the monotonic (U_{mon}) and cyclic (U_{cyc}) strain energy, as depicted in Fig. 5. The monotonic energy is the amount of strain energy stored in the specimen when d_{min} is reached in the first loading cycle. Since the displacement is never lower than d_{min} during the entire fatigue test, U_{mon} is never recovered. The cyclic energy is the amount of strain energy stored in the specimen during the loading section of the cycle due to the external work applied by the machine and recovered during the unloading section of the cycle [8]. The total strain energy (U_{tot}) correlates with G_{max} and provides a measure of the resistance to crack propagation, while U_{cyc} corresponds to the applied work and correlates with ΔG ($\Delta G = G_{max} - G_{min}$), providing a measure of the amount of energy available for crack growth

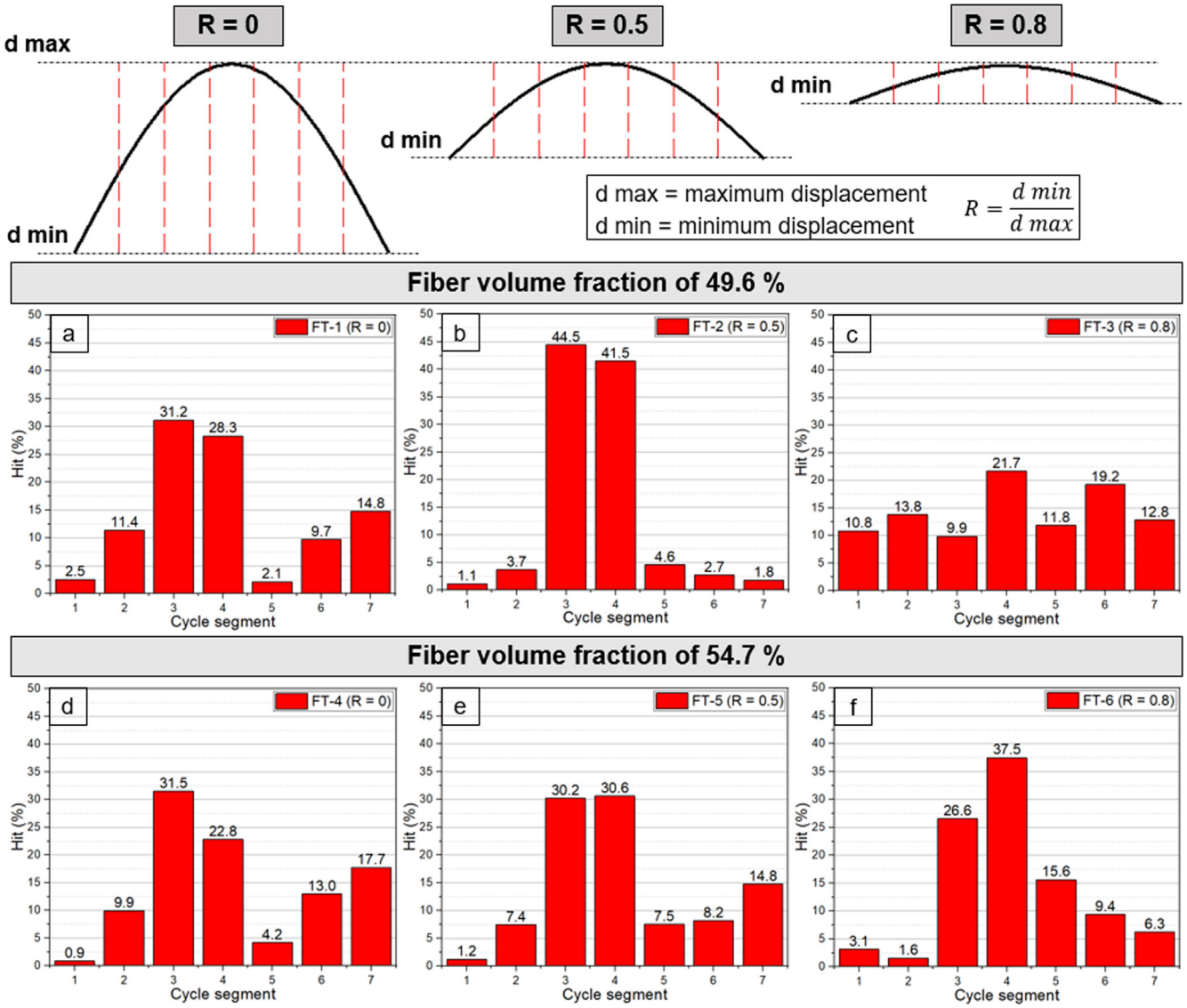

Fig. 3. Distribution of the hits within a single loading cycle of the first five hundred fatigue cycles. (For interpretation of the references to colour in this figure legend, the reader is referred to the web version of this article.)

[36]. Thus, the reduction of U_{cyc} means reducing both the external work and ΔG, leading to a reduction of the energy available for crack propagation and, consequently, a reduction of the crack propagation rate [37].

The damage propagation at the unloading stage was observed in all tests, as depicted in Figs. 3 and 4. Therefore, although most of the damage develops during the loading section of the cycle, the damage creation is not limited to the loading process. As long as U is higher than U_{th}, the damage can propagate even during the unloading. In view of physics, one can take the analogy of pulling a box over the ground, where static friction has to be overcome first before the box starts sliding, where after the peak load reaches its maximum and reduces the box still slides because the force still exceeds the (now: kinetic) friction. The increase of the R-ratio observed in the results, obtained by the increase of d_{min} while maintaining d_{max} constant led to a higher fraction of the loading cycle being in an energy state above U_{th}, enabling the damage formation during a broader region of the cycle, as can be seen in the illustrative scheme of Fig. 6.

The more homogeneous damage distribution along the fatigue cycle observed in high R-ratio tests does not mean that more damage is created when the R-ratio is increased in displacement-controlled tests, leading to higher delamination propagation rates. On the contrary, the R-ratio increase with d_{max} kept constant resulted in a decrease of the delamination propagation rate in the fatigue tests. The main reason that explains this behavior is the discontinuity of damage propagation in fatigue caused by the reduction of the external work applied to the specimen, which is discussed in Section 3.3.

3.2. Damage onset within a single loading cycle

Several hits can be detected within a single loading cycle, meaning a damage initiation followed by its propagation. Considering this, Fig. 7 displays only the first hit detected in each loading cycle to study the damage onset.

The assessment of the results presented in Fig. 7 shows that the R-ratio reduction leads to a damage onset in the early stages of the fatigue cycle, which might seem unexpected at first considering that the specimens with high R-ratios are continuously in higher levels of strain energy. For example, the strain energy state of specimen FT-2 (Fig. 7b) in sections 1 and 2 is higher than the strain energy state of specimen FT-1 (Fig. 7a) in section 2 (observation based on the increase of d_{min}). However, most of the damage onset in Fig. 7b is concentrated only in

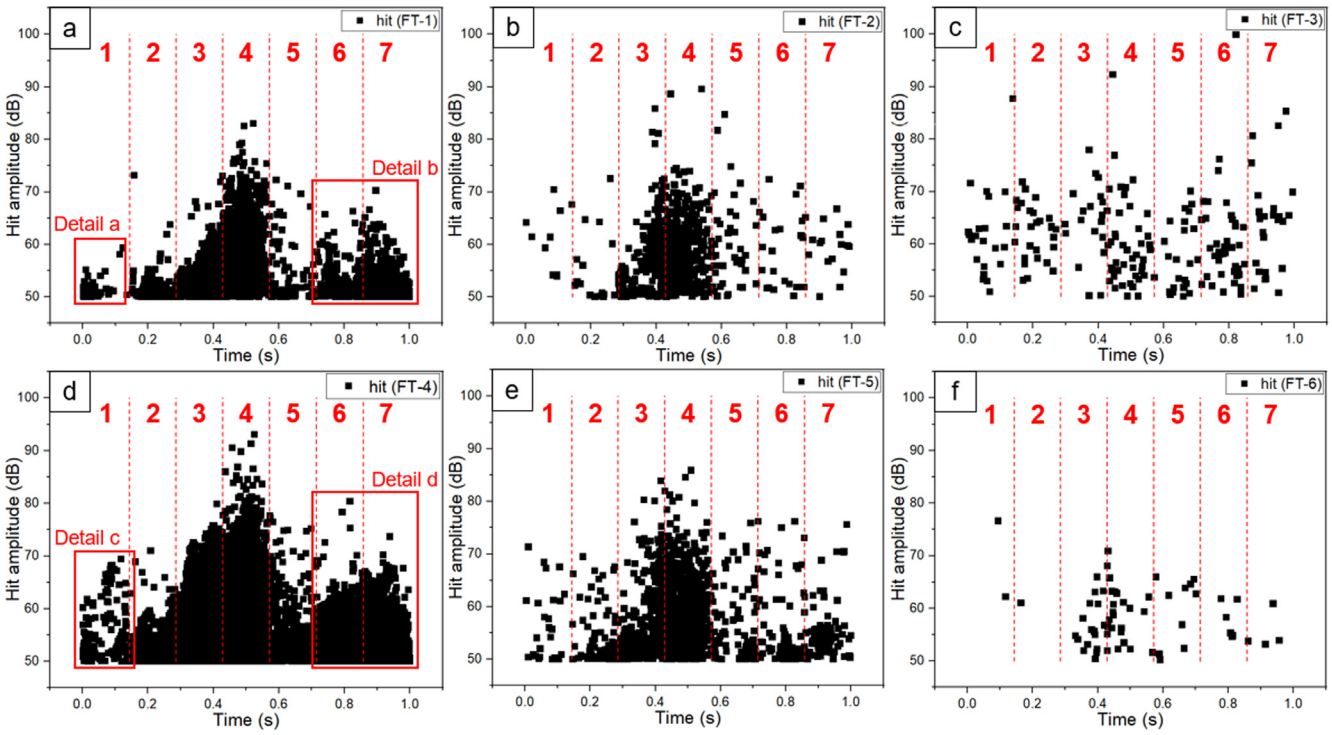

Fig. 4. Hit amplitude and distribution of the hits within a single loading cycle of the first five hundred fatigue cycles. (For interpretation of the references to colour in this figure legend, the reader is referred to the web version of this article.)

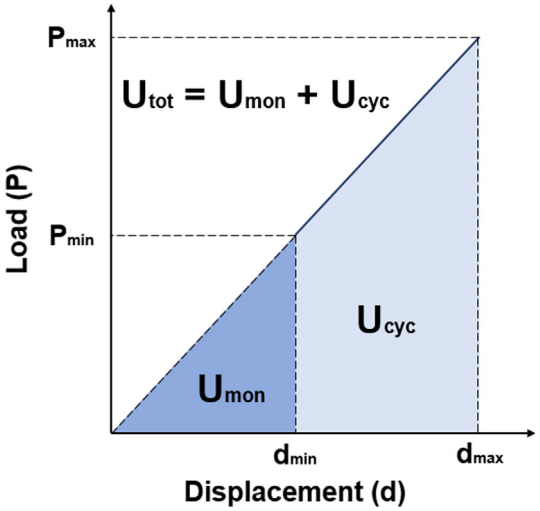

Fig. 5. Schematic diagram of load (P) versus displacement (d) with the definitions of U, U_{mon} and U_{cyc}. (For interpretation of the references to colour in this figure legend, the reader is referred to the web version of this article.)

section 3 (Fig. 7b), while the damage onset of specimen FT-1 is concentrated in section 2 (Fig. 7a). In terms of maximum strain energy (considering both monotonic and cyclic energy), these results indicate that specimen FT-2 needed more energy for damage onset in most of the cycles than specimen FT-1. Nevertheless, the U_{cyc} in section 2 of specimen FT-1 (Fig. 7a) and in section 3 of specimen FT-2 (Fig. 7b) are expected at the comparable level considering that the cyclic energy reduces when the R-ratio increases (Fig. 8).

Assuming that U_{th} is constant for specimens of the same laminate, the damage onset in section 2 (Fig. 7a) of specimen FT-1 (R = 0) indicates that specimen FT-3 (R = 0.8) is always in an energy state above U_{th}, as illustrated in Fig. 6. The same analogy can be performed for specimens FT-4 and FT-6. Thus, if damage onset exclusively depended on U_{th} and if U_{th} was unique and constant, all the damage onset observed in specimens FT-3 (Fig. 7c) and FT-6 (Fig. 7f) should be located in section 1, since the entire cycle is above U_{th}. However, an increased scatter in the damage onset and a high incidence of hits in section 4 of specimens FT-3 (Fig. 7c) and FT-6 (Fig. 7f) were observed.

The damage onset in the early stages of the fatigue cycle with the reduction of the R-ratio observed in Fig. 7 might be related to the variation of the external work applied to the specimen. The amount of

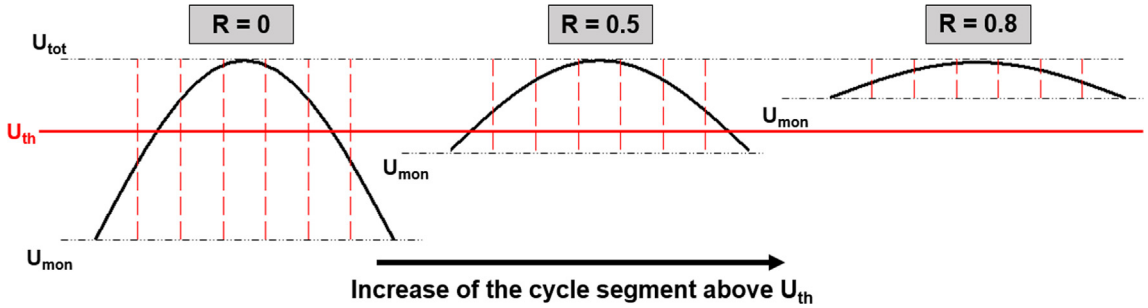

Fig. 6. Scheme of the increase of the cycle segment above U_{th} when the R-ratio increases. (For interpretation of the references to colour in this figure legend, the reader is referred to the web version of this article.)

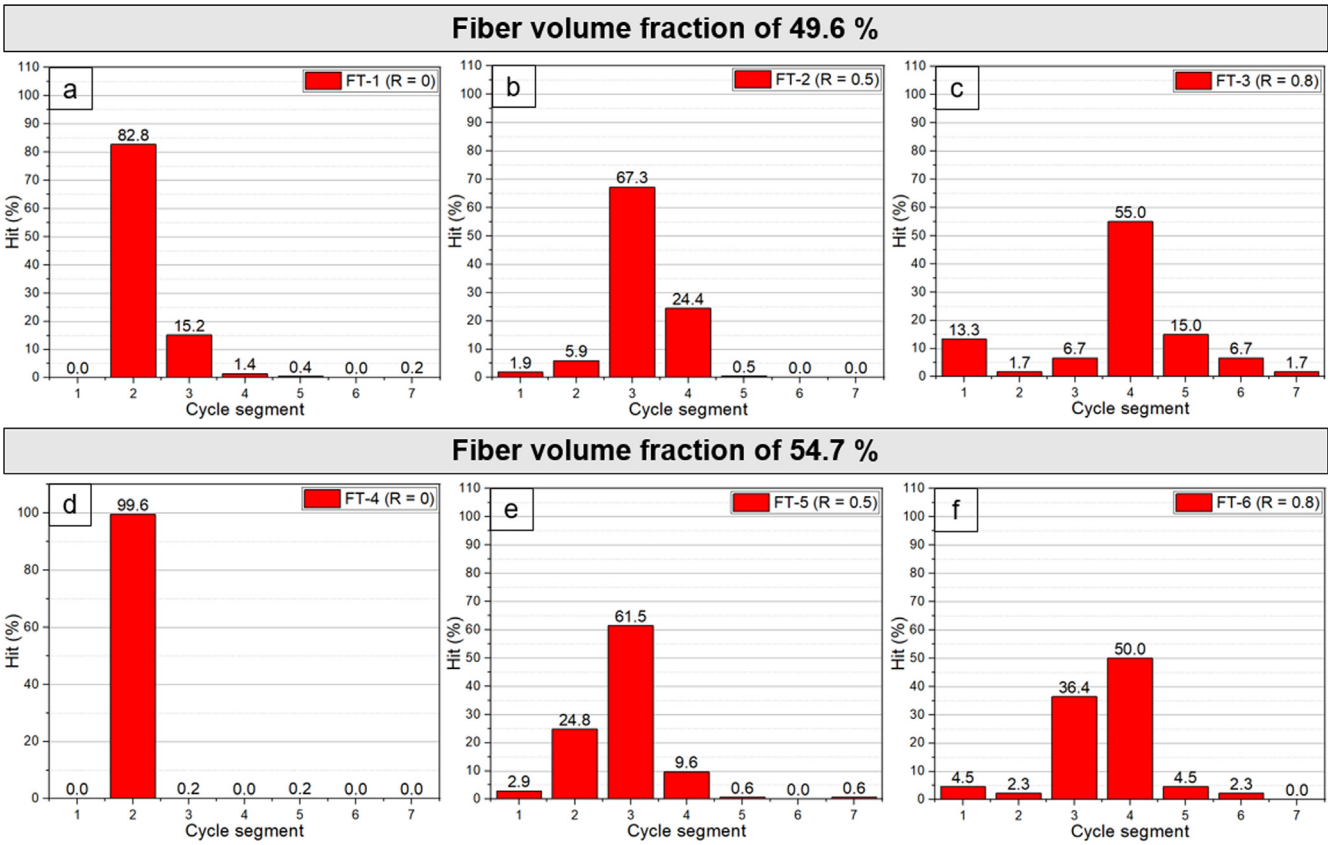

Fig. 7. Distribution of the first hits in each loading cycle during the first five hundred fatigue cycles (the hits detected in section 1 of the specimens FT-1 and FT4 were not considered as damage onset). (For interpretation of the references to colour in this figure legend, the reader is referred to the web version of this article.)

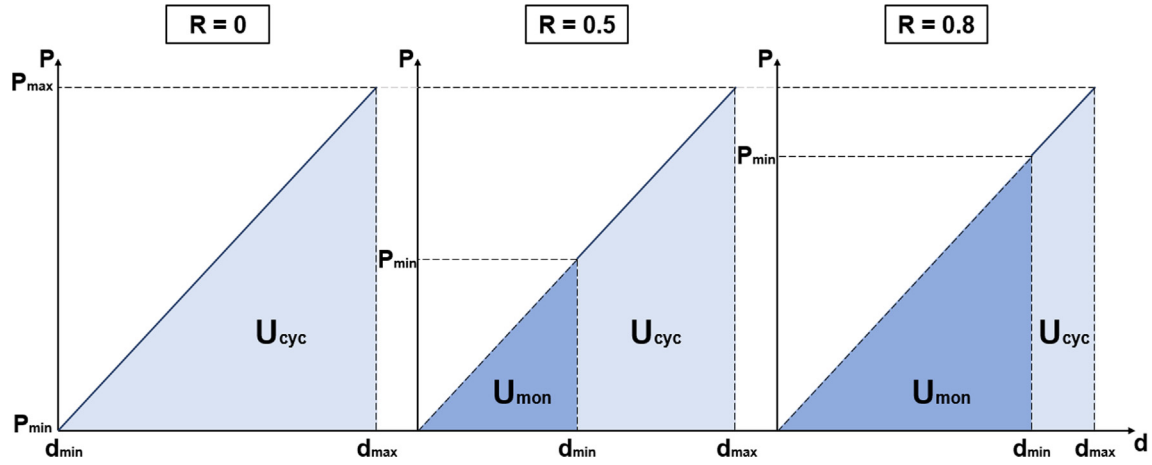

Fig. 8. Monotonic and cyclic strain energy applied to the specimen during the fatigue cycles. (For interpretation of the references to colour in this figure legend, the reader is referred to the web version of this article.)

cyclic strain energy stored in the specimen is reduced when the R-ratio is increased keeping d_{max} constant due to the reduction of the external work applied, as depicted in Fig. 8. Therefore, the cyclic strain energy stored in specimen FT-1 (R = 0) in section 2 might be equivalent to the cyclic strain energy stored in specimens FT-2 (R = 0.5) and FT-3 (R = 0.8) only in sections 3 and 4, respectively. This reveals a trend between U_{cyc} and the section of the cycle where most of the damage onset occurred, as can be seen in Fig. 7.

Considering the energy balance in which damage propagates only when the energy available (U) is equal or higher than the material's resistance (U_{th}), the strain energy level during the damage onset is equivalent to U_{th}, and its scatter also indicates a scatter of U_{th}. The results presented in Fig. 7 show a U_{th} scatter, as observed in the work of Pascoe [10], mainly in specimens with high R-ratios. Therefore, U_{th} is not constant, and the variation of U_{cyc} affects the damage onset and has some relation to U_{th}. This could be explained by a cyclic energy threshold requirement for damage formation instead of U_{th}. The influence of the U_{cyc} on the damage onset inhibits a precise determination of U_{th}. Then, U_{th} might not be considered as a unique value, but as an interval in which the likelihood of damage propagation depends on the amount of cyclic work applied to the specimen.

Table 2
Number of cycles with no hit detection and the average number of hits detected in the first 500 cycles excluding cycles without hits.

Specimen	R-ratio	Number of cycles with no hit detection	Average number of hits per cycle not considering cycles with no hit detection	Standard deviation
FT-1[1]	0.0	13	7.14	2.88
FT-2	0.5	77	2.10	1.74
FT-3	0.8	406	3.38	5.08
FT-4[1]	0.0	0	23.16	3.40
FT-5	0.5	9	4.32	2.87
FT-6	0.8	455	1.39	0.77

[1] In order to avoid any influence of noise in the analysis, the hits of sections 1, 6 and 7 (Fig. 3a and d) of the specimens FT-1 and FT-4 were excluded.

3.3. Discontinuity of damage propagation in fatigue of FRP

According to the definition of da/dN (delamination growth rate) and the results presented in Figs. 3, 4, and 7, it is possible to note the discontinuity of delamination growth in fatigue. First, the damage propagation was discontinued within a single loading cycle, as presented in Figs. 3, 4, and 7. Moreover, da/dN is defined as the crack increment developed during a single loading cycle, which means that da/dN is not continuous by definition considering a sequence of loading cycles.

The methodology employed by well-established models for FDG predictions to calculate da/dN results in approximations [1–4]. The determination of da/dN is usually conducted averaging the damage formation of successive fatigue cycles in pre-defined intervals of 100, 1000, or even 10,000 cycles leading to an apparent constant delamination growth rate in this period, which is a simplified approximation. In addition, these models also assume that delamination growth is continuous within a single loading cycle. These approximations lead to a misinterpretation of damage development during fatigue, because damage development discontinuity is hidden, as also observed in the work of Alderliesten et al. [9]. Table 2 shows the average values of the number of hits detected over the first 500 cycles of each fatigue test and the number of cycles with no hit detection.

The results presented in Table 2 show a trend of the R-ratio with both the number of cycles with no hit detection, and the average number of hits detected per cycle. The R-ratio increase reduced the external work applied to the specimen (Fig. 8), resulting in more cycles with no hit detection and a reduction of the average number of hits detected per cycle, as observed in Table 2. The absence of hits detection is interpreted as no damage propagation in these cycles, indicating an increase in damage propagation discontinuity. The high hit detection rate within a single cycle suggests that more damage mechanisms are under development simultaneously due to the high external work applied.

In order to confirm that the hits correctly represent damage propagation in fatigue tests, Fig. 9 presents curves of ΔP_{max} ($\Delta P_{max} = P_{max,\ first\ cycle} - P_{max,\ N}$) versus the number of cycles (N), and the propagated crack length versus the number of cycles.

Fig. 9b and 9d present a macro-crack length increase when the R-ratio decreases, which is in agreement with the results presented in Table 2. Even for comparisons between specimens tested with the same R-ratio, such as the specimens FT-1 and FT-4 (R = 0), the AE results and the macro-crack length showed a consistent correlation. Specimen FT-1 presented the highest average number of hits per cycle in Table 2, and also presented the most extended macro-crack length in Fig. 9d, which proves the AE technique efficiency in quantifying damage in fatigue.

The damage propagated within a single loading cycle leads to the release of a fraction of the total strain energy accumulated in the specimen, avoiding a total recovery of the cyclic energy during the unloading. Because of this, the maximum strain energy reached is reduced in the subsequent cycles, yielding a reduction of P_{max}, since d_{max} is constant. Fig. 9a and c present the reduction of P_{max} in each test caused by the damage propagation. However, specimen FT-3 showed an unexpected increase of P_{max}. A slight reduction of P_{max} was expected for specimen FT-3 since the damage propagation detected was low, similar to the behavior observed in specimen FT-6, which was tested in the same conditions (R = 0.8). The explanation for this outlier is the inability of the test machine to keep d_{max} constant during the specimen FT-3 test. Fig. 9e shows that d_{max} increased, leading to the P_{max} increase observed in Fig. 9a. Specimen FT-3 also can be considered an outlier in the results of the average number of hits per cycle, as seen in Table 2. Specimen FT-3 (R = 0.8) presented a higher number of hits per cycle than specimen FT-2 (R = 0.5), even with an R-ratio increase.

On the other hand, the increase in the number of hits per cycle observed in specimen FT-3 might be explained by the high strain energy conditions caused by the high R-ratio applied. As already discussed, the increase of d_{min} in high R-ratios increases the region of the cycle above U_{th}, which may lead to a more extended damage propagation after its onset within the cycle compared to low R-ratios. The process of subsequent damage propagation after the damage onset takes more time to stop for high R-ratios since the reduction of the elastic strain energy stored in the specimen caused by the unloading is lower compared to low R-ratios.

Therefore, for high R-ratios, more time in the loading cycle is spent above U_{th}, but the likelihood of triggering a delamination increment is lower, because of the reduced cyclic work compared to low R-ratios. Hence fewer cycles with hits are detected, but once damage propagation is triggered, it certainly continues over a larger portion of the loading cycle. Considering low R-ratios, less time in the loading cycle is above U_{th}, but with more external work. Then, the likelihood of triggering a delamination increment is higher, and the damage propagation stops more quickly within the cycle than in high R-ratios. However, the damage propagation during a shorter region of the cycle does not necessarily mean a lower damage propagation rate.

3.4. Scatter of U_{th}

In displacement-controlled conditions, the elastic strain energy available for delamination propagation is maximum in the first cycle and reduces after damage propagation. Then, if U_{th} was the only parameter needed to be overcome to enable damage formation, once no damage appears in a cycle, the damage should not take place after that. This behavior is expected because the maximum energy of the subsequent cycles will not increase due to the displacement-controlled conditions. On the other hand, according to the results presented in Table 2 and the work of Alderliesten et al. [9], the AE results indicated that the delamination could propagate in fatigue even after a sequence of cycles without the detection of any damage mechanism.

The delamination propagation process obeys an energy balance concept, in which the elastic strain energy available for delamination needs to be higher than the material's resistance (U_{th}) to enable damage formation. However, U_{th} was not constant, as can be observed in Fig. 7, and might be affected by some factors, as follows:

- Stochastic mechanisms accumulated during the loading cycles might reduce the strain energy required for damage formation. Thus, this "activation energy" drops, enabling the creation of damage;
- The presence of any defect in the specimen such as porosity and resin pockets due to the manufacturing process;
- The occurrence of different fracture modes during FDG, such as matrix cracking, fiber breakage, and interfacial failure due to the composites' heterogeneous nature. These types of failure might need a different amount of elastic strain energy to occur [23]. As there is no specific order for the development of these damage modes, the first damage event detected in the loading cycle could be any of

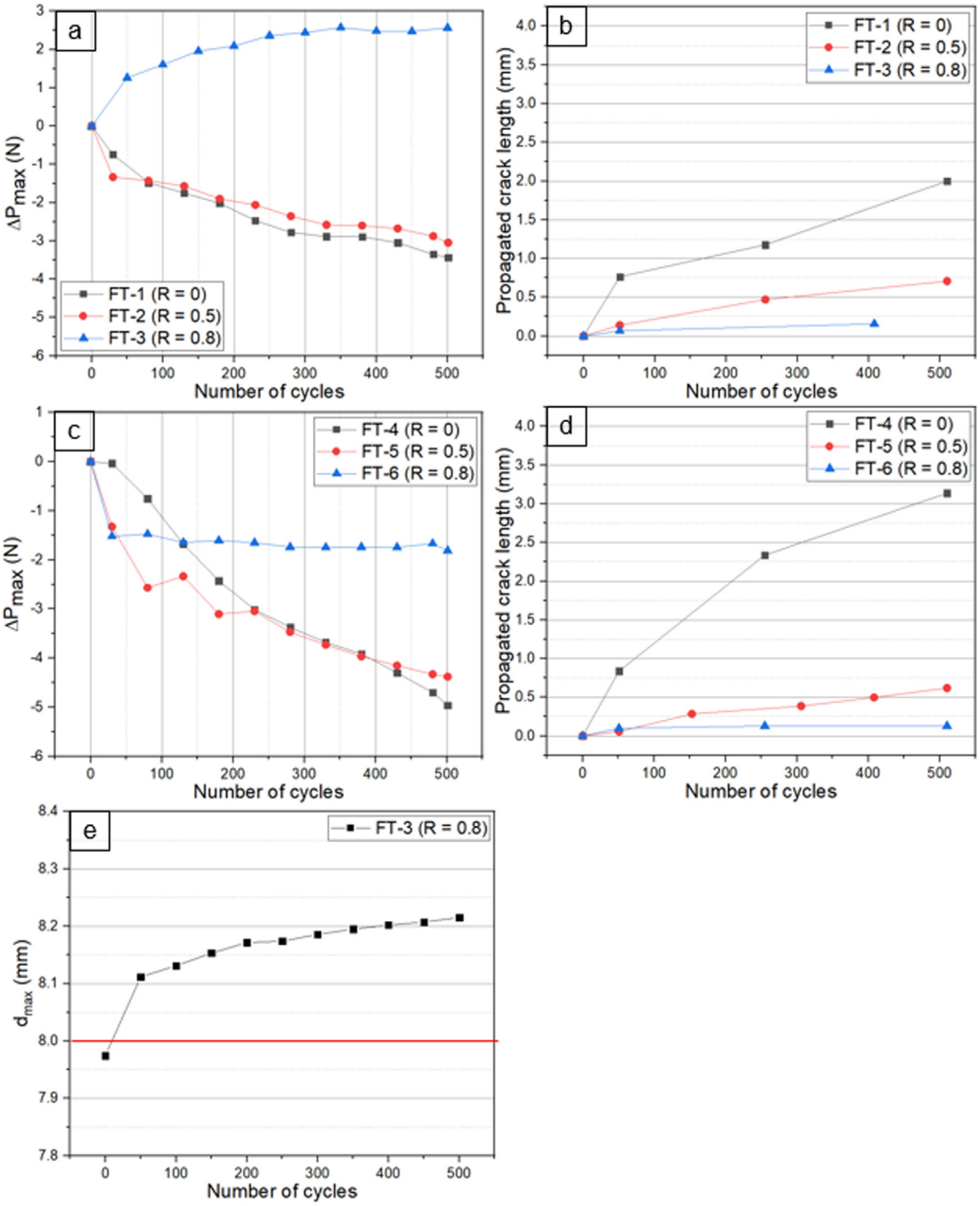

Fig. 9. First five hundred cycles: (a), (c) ΔP_{max} (defined as $P_{max,\ first\ cycle} - P_{max,\ N}$) reduction; (b), (d) crack length propagation; (e) variation of the maximum displacement. (For interpretation of the references to colour in this figure legend, the reader is referred to the web version of this article.)

these modes or a combination of them, resulting in different values of U_{th} increasing its scatter.

In the present work, the authors propose that the stochastic mechanisms are mainly related to the stress state and the damage formation ahead of the crack tip. In mode I fatigue delamination propagation conditions, the crack tip inside the specimen originates a process zone ahead of the crack tip in which the stress field is more intense than in the rest of the material. Micro-cracks and plastic deformations are accumulated in this process zone during the cyclic loading due to the high-stress conditions [14,23], as illustrated in Fig. 10a.

In case of the strain energy accumulated in the specimen (U) is lower than the U_{th} for crack propagation, the crack propagation will only occur by the coalescence of the micro-cracks ahead of the crack tip, as presented in Fig. 10b. This statement's basis relies on the fact that the crack propagation through micro-crack coalescence requires less energy than the usual crack propagation, which can be an explanation for the delamination propagation after several cycles without damage detection observed in the results. Therefore, when U is not high enough to enable crack propagation, the crack stops its propagation, and only damage mechanisms ahead of the crack tip are developed and detected by the AE system. Once the region ahead of the crack tip accumulated enough damage, the crack propagates through micro-crack coalescence consuming a lower amount of energy, which can be interpreted as a lower U_{th}.

The crack propagation through micro-crack coalescence increases the U_{th} scatter since both the micro-crack formation and the crack propagation require different amounts of energy to develop (different

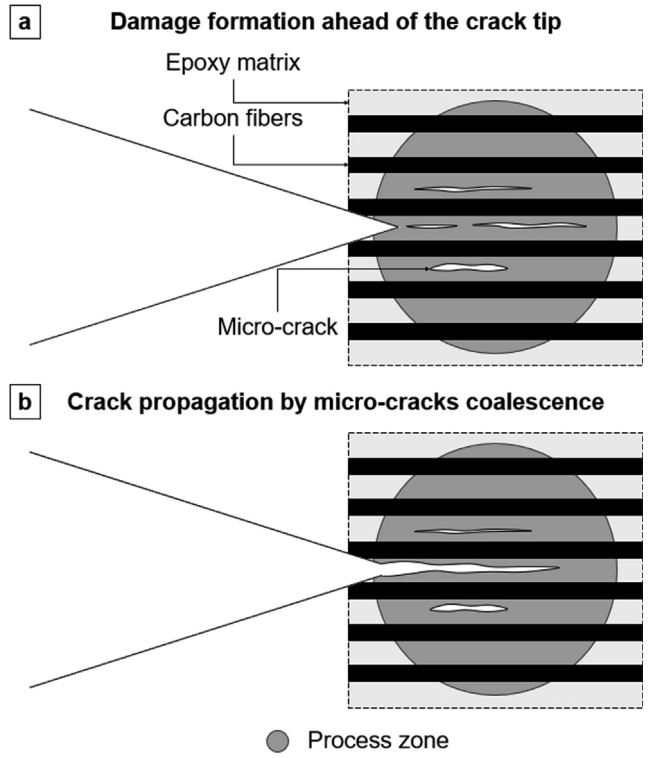

Fig. 10. Idealized illustrative scheme of the process of damage accumulation ahead of the crack tip.

U_{th}). A high U_{th} scatter is expected to be observed in low crack propagation rates in which the energy available for damage propagation (U) can be lower than the threshold energy required for the macro-crack propagation. A condition that was observed in this work when the R-ratio was increased. Thus, the R-ratio increase led to a reduction of the crack propagation rate and an increase of the U_{th} scatter, as can be observed in the results presented in Fig. 9b and d, and Fig. 7, respectively.

This section explained the scatter observed in U_{th} results based on the different amounts of energy required for the activation of different damage mechanisms, resulting in different U_{th}. It is reasonable to assume that each one of these damage mechanisms requires a specific amount of energy to develop despite the R-ratio applied. Therefore, why does the U_{th} showed an increase in the results presented in Fig. 7 when the R-ratio was increased, maintaining d_{max} constant? The response to this question relies on the cyclic strain energy applied, as discussed in Section 3.2. Thus, the threshold of strain energy required for damage onset within a single loading cycle in fatigue might relate better with U_{cyc} than with U_{th}, since U_{th} considers both U_{mon} and U_{cyc} energies.

4. Conclusions

The capability of the AE technique to quantify physical damage in FDG was evaluated in this work. Based on the results presented, the AE technique proved to be suitable to evaluate the damage formation during fatigue loadings, providing insight into the mechanisms of delamination propagation.

The analysis of damage distribution in the course of a single loading cycle, and the assessment of damage development cycle by cycle enabled the following statements about FDG:

- Damage is developed during both loading and unloading phases of the fatigue cycle;
- The damage developed during the unloading is generally a consequence of any damaging event initiated during the loading;
- The R-ratio directly relates to the external work applied to the specimen, which changes both the damage distribution within a single loading cycle and the continuity of damage development cycle by cycle;
- A threshold level of energy (U_{th}), which is the material's resistance, needs to be overcome in each loading cycle to enable damage propagation. However, the cyclic strain energy showed a strong correlation with the results and, possibly, a cyclic strain energy threshold might be considered as a condition to damage formation instead of U_{th};
- The increase of the R-ratio leads to a larger fraction of the loading cycle being above U_{th}, which means that damage mechanisms can develop along a broader region of the loading cycle;
- The damage onset within a single loading cycle correlates with the cyclic strain energy of the specimen. Thus, the R-ratio variation indirectly correlates with the damage onset;
- The increase of the R-ratio reduces the likelihood of triggering damage propagation because the external work reduces, reducing the delamination propagation continuity;
- The U_{th} scatter is caused by the presence of different damaging processes during the delamination propagation, which require a different amount of energy to occur (different U_{th}), such as micro-crack formation ahead of the crack tip, micro-crack coalescence and crack propagation;
- The FVF evaluated in this work did not present as an essential influence on the results.

The delamination process in fatigue, when physically explained, enables the development of more precise prediction models based on micromechanics. Therefore, future works should continue to investigate the FDG mechanisms aiming to increase the physical understanding of the phenomenon to enable the creation of reliable micromechanical models.

CRediT authorship contribution statement

Roberto Motta: Conceptualization, Methodology, Validation, Formal analysis, Investigation, Data curation, Writing - original draft, Writing - review & editing, Visualization, Funding acquisition. **René Alderliesten:** Conceptualization, Formal analysis, Writing - original draft, Writing - review & editing, Supervision, Resources. **Marcos Shiino:** Conceptualization, Formal analysis, Writing - original draft, Writing - review & editing, Supervision. **Maria Odila Cioffi:** Resources, Supervision, Project administration. **Herman Voorwald:** Conceptualization, Writing - original draft, Project administration.

Declaration of Competing Interest

The authors declare that they have no known competing financial interests or personal relationships that could have appeared to influence the work reported in this paper.

Acknowledgement

The authors acknowledge the financial support by FAPESP, through process numbers 2015/15288-5, 2017/03698-0, and 2019/00846-3, and by Coordenação de Aperfeiçoamento de Pessoal de Nível Superior - Brasil (CAPES) - Finance Code 001.

References

[1] Amaral L, Yao L, Alderliesten R, Benedictus R. The relation between the strain energy release in fatigue and quasi-static crack growth. Eng Fract Mech 2015;145:86–97. https://doi.org/10.1016/j.engfracmech.2015.07.018.
[2] Zhang B, Kawashita LF, Hallett SR. Composites fatigue delamination prediction

using double load envelopes and twin cohesive models. 105711 Compos Part A Appl Sci Manuf2019. https://doi.org/10.1016/j.compositesa.2019.105711.
[3] Yao L, Alderliesten RC, Jones R, Kinloch AJ. Delamination fatigue growth in polymer-matrix fibre composites: a methodology for determining the design and lifing allowables. Compos Struct 2018;196:8–20. https://doi.org/10.1016/j.compstruct.2018.04.069.
[4] Jones R, Pitt S, Bunner AJ, Hui D. Application of the Hartman-Schijve equation to represent Mode I and Mode II fatigue delamination growth in composites. Compos Struct 2012;94:1343–51. https://doi.org/10.1016/j.compstruct.2011.11.030.
[5] Khan R, Alderliesten R, Benedictus R. Two-parameter model for delamination growth under mode I fatigue loading (Part A: Experimental study). Compos Part A Appl Sci Manuf 2014;65:190–200. https://doi.org/10.1016/j.compositesa.2014.06.007.
[6] Varandas LF, Arteiro A, Catalanotti G, Falzon BG. Micromechanical analysis of interlaminar crack propagation between angled plies in mode I tests. Compos Struct 2019;220:827–41. https://doi.org/10.1016/j.compstruct.2019.04.050.
[7] Bertorello C, Viña J, Viña I, Argüelles A. Study of the influence of the type of matrix used in carbon-epoxy composites on fatigue delamination under mode III fracture. Mater Des 2020;186. https://doi.org/10.1016/j.matdes.2019.108345.
[8] Pascoe JA, Alderliesten RC, Benedictus R. On the relationship between disbond growth and the release of strain energy. Eng Fract Mech 2015;133:1–13. https://doi.org/10.1016/j.engfracmech.2014.10.027.
[9] Alderliesten RC, Brunner AJ, Pascoe JA. Cyclic fatigue fracture of composites: What has testing revealed about the physics of the processes so far? Eng Fract Mech 2018;203:186–96. https://doi.org/10.1016/j.engfracmech.2018.06.023.
[10] Pascoe JA, Zarouchas DS, Alderliesten RC, Benedictus R. Using acoustic emission to understand fatigue crack growth within a single load cycle. Eng Fract Mech 2018;194:281–300. https://doi.org/10.1016/j.engfracmech.2018.03.012.
[11] Khan R, Alderliesten R, Benedictus R. Two-parameter model for delamination growth under mode I fatigue loading (Part B: Model development). Compos Part A Appl Sci Manuf 2014;65:201–10. https://doi.org/10.1016/j.compositesa.2014.06.008.
[12] Brighenti R, Carpinteri A, Scorza D. Micromechanical crack growth-based fatigue damage in fibrous composites. Int J Fatigue 2016;82:98–109. https://doi.org/10.1016/j.ijfatigue.2015.04.007.
[13] Yao L, Alderliesten RC, Zhao M, Benedictus R. Discussion on the use of the strain energy release rate for fatigue delamination characterization. Compos Part A Appl Sci Manuf 2014;66:65–72. https://doi.org/10.1016/j.compositesa.2014.06.018.
[14] Khan R, Alderliesten R, Badshah S, Khattak MA, Khan MS, Benedictus R. Experimental investigation of the microscopic damage development at mode i fatigue delamination tips in carbon/epoxy laminates. J Teknol 2016;78:33–40https://doi.org/10.11113/.v78.8072.
[15] Barile C, Casavola C, Pappalettera G, Vimalathithan PK. Damage characterization in composite materials using acoustic emission signal-based and parameter-based data. Compos Part B Eng 2019;178:107469https://doi.org/10.1016/j.compositesb.2019.107469.
[16] Kelkel B, Popow V, Gurka M. Inline quantification and localization of transverse matrix cracking in cross-ply CFRP during quasi-static tensile testing by a joint event-based evaluation of acoustic emission and passive IR thermography. Compos Sci Technol 2020;190:108013https://doi.org/10.1016/j.compscitech.2020.108013.
[17] Murray BR, Kalteremidou KA, Carrella-Payan D, Cernescu A, Van Hemelrijck D, Pyl L. Failure characterisation of CF/epoxy V-shape components using digital image correlation and acoustic emission analyses. Compos Struct 2020;236:111797https://doi.org/10.1016/j.compstruct.2019.111797.
[18] Mi Y, Zhu C, Li X, Wu D. Acoustic emission study of effect of fiber weaving on properties of fiber-resin composite materials. Compos Struct 2020;237. https://doi.org/10.1016/j.compstruct.2020.111906.
[19] Saeedifar M, Zarouchas D. Damage characterization of laminated composites using acoustic emission: a review. Compos Part B Eng 2020;195:108039https://doi.org/10.1016/j.compositesb.2020.108039.
[20] Sause M, Hamstad M. Acoustic emission analysis 2017;vol. 7. https://doi.org/10.1016/B978-0-12-803581-8.10036-0.
[21] Barile C, Casavola C, Pappalettera G, Vimalathithan PK. Experimental wavelet analysis of acoustic emission signal propagation in CFRP. Eng Fract Mech 2019;210:400–7. https://doi.org/10.1016/j.engfracmech.2018.05.030.
[22] Oz FE, Ersoy N, Lomov SV. Do high frequency acoustic emission events always represent fibre failure in CFRP laminates? Compos Part A Appl Sci Manuf 2017;103:230–5. https://doi.org/10.1016/j.compositesa.2017.10.013.
[23] Sause MGR, Müller T, Horoschenkoff A, Horn S. Quantification of failure mechanisms in mode-I loading of fiber reinforced plastics utilizing acoustic emission analysis. Compos Sci Technol 2012;72:167–74. https://doi.org/10.1016/j.compscitech.2011.10.013.
[24] Michalcová L, Kadlec M. Carbon/epoxy composite delamination analysis by acoustic emission method under various environmental conditions. Eng Fail Anal 2016;69:88–96. https://doi.org/10.1016/j.engfailanal.2016.01.008.
[25] Saeedifar M, Fotouhi M, Ahmadi Najafabadi M, Hosseini Toudeshky H, Minak G. Prediction of quasi-static delamination onset and growth in laminated composites by acoustic emission. Compos Part B Eng 2016;85:113–22. https://doi.org/10.1016/j.compositesb.2015.09.037.
[26] Nikbakht M, Yousefi J, Hosseini-Toudeshky H, Minak G. Delamination evaluation of composite laminates with different interface fiber orientations using acoustic emission features and micro visualization. Compos Part B Eng 2017;113:185–96. https://doi.org/10.1016/j.compositesb.2016.11.047.
[27] Hamstad MA. Frequencies and amplitudes of AE signals in a plate as a function of source rise time. 29th Eur. Conf. Acoust. Emiss. Test., 2010.
[28] Barile C. Innovative mechanical characterization of CFRP by using acoustic emission technique. Eng Fract Mech 2019;210:414–21. https://doi.org/10.1016/j.engfracmech.2018.02.024.
[29] D5528-13. Standard Test Method for Mode I Interlaminar Fracture Toughness of Unidirectional Fiber-Reinforced Polymer Matrix Composites. ASTM B Stand 2013;1:1–12. https://doi.org/10.1520/D5528-01R07E03.2.
[30] Technique G, Composites T. D3171-15 Standard Test Methods for Constituent Content of Composite Materials 2000;76:1–10. https://doi.org/10.1520/D3171-15.2.
[31] D6115-97(2004). Standard Test Method for Mode I Fatigue Delamination Growth Onset of Unidirectional Fiber Reinforced Polymer Matrix Composites. ASTM B Stand 2004;97:1–6. https://doi.org/10.1520/D6115-97R11.2.
[32] Finkel P. Experimental study of “Auto Sensor Test–Self Test Mode” for Acoustic Emission system performance verification 2003;1995:1995–2002. https://doi.org/10.1063/1.1291316.
[33] ASTM-E976-15. Standard guide for determining the reproducibility of acoustic emission sensor response. Am. Soc. Test. Mater., 2015.
[34] Amaral L, Zarouchas D, Alderliesten R, Benedictus R. Energy dissipation in mode II fatigue crack growth. Eng Fract Mech 2017;173:41–54. https://doi.org/10.1016/j.engfracmech.2017.01.020.
[35] Jeong H, Hsu DK. Experimental analysis of porosity-induced ultrasonic attenuation and velocity change in carbon composites. Ultrasonics 1995;33:195–203. https://doi.org/10.1016/0041-624X(95)00023-V.
[36] Pascoe JA, Alderliesten RC, Benedictus R. On the physical interpretation of the R-ratio effect and the LEFM parameters used for fatigue crack growth in adhesive bonds 2017;97:162–76.
[37] Bak BLV, Sarrado C, Turon A, Costa J. Delamination under fatigue loads in composite laminates: a review on the observed phenomenology and computational methods. Appl Mech Rev 2014;66.. https://doi.org/10.1115/1.4027647.